Advances in Materials Research, *Vol. 15, No. 1 (2026) 83-105*
https://doi.org/10.12989/amr.2026.15.1.083

Techno-Press

Porosity effects on the thermal buckling of functionally graded plate: Modeling and analysis

Khayra Draouche*[1], Lazreg Hadji[2], Royal Madan[3], Nafissa Zouatnia[2], Hassen Ait Atmane[4]

[1]*Laboratory of Geomatics and Sustainable Development, University of Tiaret, Algeria*
[2]*Department of Civil Engineering, University of Tiaret, BP 78 Zaaroura, Tiaret, 14000, Algeria*
[3]*Department of Mechanical Engineering, Graphic Era (Deemed to be University), Dehradun 248002, Uttarakhand, India*
[4]*Laboratory of Structures, Geotechnics and Risks, Department of Civil Engineering, Hassiba Benbouali University of Chlef, Chlef, Algeria*

(Receive December 20, 2025, Revised March 5, 2026, Accepted March 10, 2026)

Abstract. Porosity in functionally graded materials (FGMs) arises during fabrication due to several factors, depending on the technique employed. The type of reinforcement used significantly influences the overall porosity percentage. The presence of porosity negatively affects the performance of FG structures. Consequently, this study focuses on conducting a thermal buckling analysis of FG porous plates using a refined shear deformation plate theory. This theory accounts for a quadratic variation of the transverse shear strains through the thickness and satisfies zero traction boundary conditions on the plate's top and bottom surfaces without relying on shear correction factors. Thermal loads were applied by varying the temperature uniformly, linearly, and non-linearly through the thickness. The problem was addressed assuming the plate to be simply supported at its ends. The rule of mixtures was used to estimate the material properties, and a porosity parameter was introduced to represent the equal distribution of porosity in the metal and ceramic mixture. The effects of volume fraction index, porosity fraction index, aspect ratio, and side-to-thickness ratio were investigated.

Keywords: FG plate; functionally graded materials; porosity; refined shear deformation plate theory; thermal buckling

1. Introduction

A functionally graded (FG) structure ultimately possesses a high strength-to-weight ratio along with excellent wear resistance, which makes it highly attractive for various industrial applications [1]. The fabrication of FGMs can be classified into solid-phase, liquid-phase, and gas-phase processes. In some processes, a layer-wise graded material is produced, while in others, a continuous gradation is achieved. It has been observed that the addition of reinforcement increases porosity in FGMs, particularly when the particles have irregular shapes [2, 3]. The effect of graphene platelets (GPLs) was examined by conducting a thermo-elastic analysis of cylindrical panels for various distributions, revealing that a slight increase in GPL content leads to reduced

*Corresponding author, Ph.D., E-mail: khayra.draouche@univ-tiaret.dz

ISSN: 2234-0912(Print), 2234-179X (Online)

displacement [4]. Copper-alumina-graded FGMs were fabricated using spark plasma sintering; the study examined the impact of reinforcement and its size, and findings show an increase in reinforcement size leads to higher porosity in the FGM [5]. A nickel-alumina-reinforced FGM was produced using the microwave sintering technique, and a porosity analysis showed higher porosity percentages as the metal composition increased [6]. An aluminum-based carbon nanotube (CNT) reinforced FGM was developed using the powder metallurgy method, where an increase in CNT composition resulted in a decrease in overall density [7].

A metal-rich FG structure exhibits lower stress magnitudes and helps prevent ceramic cracking [8]. For a 2D FG plate, a differential transform method combined with shear deformation theory was utilized to perform free vibration analysis [9]. Free vibration analysis of FG porous plates with cutouts was conducted using an FE-based multilayered FGM model, which accounted for the effects of various porosity distributions on vibration behavior, demonstrating the model's effectiveness in analyzing complex FGM structures [10]. A first-order shear deformation theory (NFSDT) for functionally graded plates was developed, requiring fewer unknowns compared to traditional theories. This approach accurately predicts bending and dynamic behaviors, simplifying analysis without stretching-bending coupling effects [11]. Static analysis of functionally graded plates with porosities was performed using a refined plate theory, considering parabolic shear stress distribution [12]. Free vibration analysis of a circular plate made of functionally graded material with piezoelectric layers was conducted using classical plate theory. Analytical solutions were compared with finite element results, examining the effects of boundary conditions [13]. A refined quasi-three-dimensional shear deformation theory was developed for the thermo-mechanical analysis of functionally graded sandwich plates on a Pasternak elastic foundation. With only four unknowns, it accurately accounts for stretching effects and satisfies boundary conditions [14]. Buckling analysis of a simply supported FG plate was performed, studying the influence of different loading and material grading indices using Navier’s method [15]. Buckling analysis of an open-edge crack beam was conducted using the finite element method with graphene as reinforcement. The study found that a higher GPL distribution at the top increases the buckling load Similar analysis was performed using Timoshenko beam theory, investigating the effects of material gradations and geometrical parameters [16].

Free vibration and stability analysis of even and uneven porous FG nano-composite cylindrical panels was performed. Hamilton’s principle was utilized for uniform and non-uniform in-plane loads [17]. The virtual principle was employed to investigate the buckling analysis of the FG sandwich plate under different boundary conditions subjected to nonlinear thermal loading [18]. Love–Kirchhoff hypothesis was utilized to solve the buckling problem for a porous plate where it is assumed that the pores of the foam are filled with fluid; the effect of porosity distribution was then investigated under thermal loading [19]. Many pieces of research have been performed in solving the buckling problems by employing various techniques such as the finite element model [20], isogeometric analysis [21, 22], generalized differential quadrature method [23], Navier solution [24], mesh free method [25], sinusoidal shear deformation plate theory [26], strain gradient higher-order theories [27], Reissner's shell theory [28] first-order shear deformation theory [29], higher order finite element model [30], nonlocal strain gradient elasticity theory [31] etc to name a few.

In this study, the thermal buckling behavior of imperfect functionally graded plates with porosities is analyzed. A refined shear deformation plate theory is proposed, which accounts for both bending and shear effects. The equilibrium and stability equations are derived based on this theory. To illustrate the effects of volume fraction index, porosity fraction index, and geometry on

the buckling temperature difference of defective FG plates, an extensive parametric analysis was conducted. The study's validation was performed using the present method, examining the influence of parameters such as the power-law index, length-to-thickness ratio, and porosity parameters on buckling. The literature review on the fabrication of Functionally graded materials (FGMs) highlights the development of porosity and its underlying causes. Porosity in FGMs varies with fabrication methods and associated parameters. In this study, it is assumed that the porosity distribution is uniform within the metal and ceramic phases. The temperature change is considered in three forms: uniform, linear, and non-linear.

2. Problem formulation

2.1 Constitutive relations of (metal/ceramic) functionally graded plates

Taking into account an imperfect FGM with a porosity volume percentage that is equally distributed between the metal and ceramic,β (β<<1), the modified rule of mixture was proposed by [32] is given by:

$$P = P_m\left(V_m - \frac{\beta}{2}\right) + P_c\left(V_c - \frac{\beta}{2}\right) \tag{1}$$

The overall composition of metal and ceramic is: $V_m + V_C = 1$ and the power law of volume fraction of the ceramic is described as Table 1

$$V_c = \left(\frac{z}{h} + \frac{1}{2}\right)^k \tag{2}$$

Employing the rule of mixture the material properties can be written as [32]:

$$\begin{aligned} E(z) &= (E_c - E_m)\left(\frac{z}{h} + \frac{1}{2}\right)^k + E_m - \frac{\beta}{2}(E_c + E_m) \\ \alpha(z) &= (\alpha_c - \alpha_m)\left(\frac{z}{h} + \frac{1}{2}\right)^k + \alpha_m - \frac{\beta}{2}(\alpha_c + \alpha_m) \\ \rho(z) &= (\rho_c - \rho_m)\left(\frac{z}{h} + \frac{1}{2}\right)^k + \rho_m - \frac{\beta}{2}(\rho_c + \rho_m) \end{aligned} \tag{3}$$

The parameter k $(0 \le k \le \infty)$ which can be either a power-law or a volume fraction index. The distance z from the FG plate's mid-plane. When k is set to zero, the FG plate becomes ceramic, while for large values, it becomes fully metal. However, Poisson's ratio (ν) is assumed to be constant. The material properties of a perfect FG plate can be obtained when β is set to zero.

As:

$$V_c + V_m = 1 \Rightarrow V_c = 1 - V_m \tag{4}$$

Type I: Perfect FG plate (Without porosity $\beta = 0$)

$$E(z) = (E_c - E_m)\left(\frac{z}{h} + \frac{1}{2}\right)^k + E_m \tag{5}$$

Type II: 50% Ceramic, 50% Metal

$$E(z) = E_m\left(V_m - \frac{\beta}{2}\right) + E_c\left(V_c - \frac{\beta}{2}\right); E(z) = (E_c - E_m)\left(\frac{z}{h} + \frac{1}{2}\right)^k + E_m - (E_c + E_m)\frac{\beta}{2} \quad (6)$$

Type III: 60% Ceramic, 40% Metal

$$E(z) = E_m\left(V_m - \frac{2\beta}{5}\right) + E_c\left(V_c - \frac{3\beta}{5}\right); E(z) = (E_c - E_m)\left(\frac{z}{h} + \frac{1}{2}\right)^k + E_m - (3E_c + 2E_m)\frac{\beta}{5} \quad (7)$$

Type IV: 40% Ceramic, 60% Metal

$$E(z) = E_m\left(V_m - \frac{3\beta}{5}\right) + E_c\left(V_c - \frac{2\beta}{5}\right); E(z) = (E_c - E_m)\left(\frac{z}{h} + \frac{1}{2}\right)^k + E_m - (2E_c + 3E_m)\frac{\beta}{5} \quad (8)$$

Type V: 75% Ceramic, 25% Metal

$$E(z) = E_m\left(V_m - \frac{\beta}{4}\right) + E_c\left(V_c - \frac{3\beta}{4}\right); E(z) = (E_c - E_m)\left(\frac{z}{h} + \frac{1}{2}\right)^k + E_m - (3E_c + E_m)\frac{\beta}{4} \quad (9)$$

Type VI: 25% Ceramic, 75% Metal

$$E(z) = E_m\left(V_m - \frac{3\beta}{4}\right) + E_c\left(V_c - \frac{\beta}{4}\right);\ E(z) = (E_c - E_m)\left(\frac{z}{h} + \frac{1}{2}\right)^k + E_m - (E_c + 3E_m)\frac{\beta}{4} \quad (10)$$

2.2 Basic Assumptions

The theory assumes the following:

(1) In comparison to plate thickness, the displacements are small and so are the strains.

(2) Shear and bending are the two components w_b and w_s that make up the transverse displacement. These elements only depend on the coordinates x and y.

$$w(x, y, z) = w_b(x, y) + w_s(x, y) \quad (11)$$

(3) Compared to in-plane stresses $\sigma_x$andσ_y the transverse normal stress$\sigma_z$is minimal.

(4) There are shear, bending, and extension components to the displacements in the x and y directions.

$$u = u_0 + u_b + u_s,\ v = v_0 + v_b + v_s \quad (12)$$

(5) It is believed that the bending components $u_b$and v_b and resemble the displacements provided by the classical plate theory. Consequently, the following can be used to convey and:

$$u_b = -z\frac{\partial w_b}{\partial x},\ v_b = -z\frac{\partial w_b}{\partial y} \quad (13)$$

(6) The shear components u_s and v_s results in parabolic change with w_s, to the parabolic variations of shear strains γ_{xz}, γ_{yz}consequently the shear stresses τ_{xz}, τ_{yz}across the plate's thickness, with the result that shear stresses are zero at the plate's top and bottom faces. As a result, the equation for and is as follows:

$$u_s = -f(z)\frac{\partial w_s}{\partial x},\ v_s = -f(z)\frac{\partial w_s}{\partial y} \quad (14)$$

where

$$f(z) = -\frac{z}{4} + \frac{5z^3}{3h^2} \tag{15}$$

2.3 Displacement Field and Strains

The Eqs. (11-15) can be used to determine the displacement field based on the assumptions made in the section before this one.

$$u(x,y,z) = u_0(x,y) - z\frac{\partial w_b}{\partial x} - f(z)\frac{\partial w_s}{\partial x} \tag{16a}$$

$$v(x,y,)z = v_0(x,y) - z\frac{\partial w_b}{\partial y} - f(z)\frac{\partial w_s}{\partial y} \tag{16b}$$

$$w(x,y,z) = w_b(x,y) + w_s(x,y) \tag{16c}$$

The following are the non-linear von Karman strain-displacement equations:

$$\begin{Bmatrix}\varepsilon_x\\ \varepsilon_y\\ \gamma_{xy}\end{Bmatrix} = \begin{Bmatrix}\varepsilon_x^0\\ \varepsilon_y^0\\ \gamma_{xy}^0\end{Bmatrix} + z\begin{Bmatrix}k_x^b\\ k_y^b\\ k_{xy}^b\end{Bmatrix} + f(z)\begin{Bmatrix}k_s^s\\ k_s^s\\ k_{xy}^s\end{Bmatrix}, \begin{Bmatrix}\gamma_{xz}\\ \gamma_{yz}\end{Bmatrix} = g(z)\begin{Bmatrix}\gamma_{xz}^s\\ \gamma_{yz}^s\end{Bmatrix} \tag{17}$$

where

$$\begin{Bmatrix}\varepsilon_x^0\\ \varepsilon_y^0\\ \gamma_{xy}^0\end{Bmatrix} = \begin{Bmatrix}\frac{\partial u_0}{\partial x} + \frac{1}{2}\left(\frac{\partial w_b}{\partial x} + \frac{\partial w_s}{\partial x}\right)^2\\ \frac{\partial v_0}{\partial y} + \frac{1}{2}\left(\frac{\partial w_b}{\partial y} + \frac{\partial w_s}{\partial y}\right)^2\\ \frac{\partial u_0}{\partial y} + \frac{\partial v_0}{\partial x} + \left(\frac{\partial w_b}{\partial x} + \frac{\partial w_s}{\partial x}\right)\left(\frac{\partial w_b}{\partial y} + \frac{\partial w_s}{\partial y}\right)\end{Bmatrix},$$

$$\begin{Bmatrix}k_x^b\\ k_y^b\\ k_{xy}^b\end{Bmatrix} = \begin{Bmatrix}-\frac{\partial^2 w_b}{\partial x^2}\\ -\frac{\partial^2 w_b}{\partial y^2}\\ -2\frac{\partial^2 w_b}{\partial x \partial y}\end{Bmatrix}, \begin{Bmatrix}k_x^s\\ k_y^s\\ k_{xy}^s\end{Bmatrix} = \begin{Bmatrix}-\frac{\partial^2 w_s}{\partial x^2}\\ -\frac{\partial^2 w_s}{\partial y^2}\\ -2\frac{\partial^2 w_s}{\partial x \partial y}\end{Bmatrix}, \begin{Bmatrix}\gamma_{xz}^s\\ \gamma_{yz}^s\end{Bmatrix} = \begin{Bmatrix}\frac{\partial w_s}{\partial x}\\ \frac{\partial w_s}{\partial y}\end{Bmatrix} \tag{18a}$$

$$g(z) = 1 - \frac{df(z)}{dz} \tag{18b}$$

2.4 Constitutive Relations

The plate is subjected to a thermal load $T(x,y,z)$. The linear constitutive relations are

$$\begin{Bmatrix}\sigma_x\\ \sigma_y\\ \tau_{xy}\end{Bmatrix} = \begin{bmatrix}C_{11} & C_{12} & 0\\ C_{12} & C_{22} & 0\\ 0 & 0 & C_{66}\end{bmatrix}\begin{Bmatrix}\varepsilon_x - \alpha T\\ \varepsilon_y - \alpha T\\ \gamma_{xy}\end{Bmatrix}, \begin{Bmatrix}\tau_{yz}\\ \tau_{xz}\end{Bmatrix} = \begin{bmatrix}C_{44} & 0\\ 0 & C_{55}\end{bmatrix}\begin{Bmatrix}\gamma_{yz}\\ \gamma_{xz}\end{Bmatrix} \tag{19}$$

where $(\sigma_x, \sigma_y, \tau_{xy}, \tau_{xz}, \tau_{yz})$ and $(\varepsilon_x, \varepsilon_y, \gamma_{xy}, \gamma_{xz}, \gamma_{yz})$ are the stress and strain components, respectively. The stiffness coefficients C_{ij} are expressed by

$$C_{11} = C_{22} = \frac{E(z)}{1-\nu^2}, \tag{20a}$$

$$C_{12} = \frac{\nu E(z)}{1-\nu^2}, \tag{20b}$$

$$C_{44} = C_{55} = C_{66} = \frac{E(z)}{2(1+\nu)}, \tag{20c}$$

2.5 Stability Equations

The FG plate's total potential energy can be expressed as

$$U = \int\int\int \begin{bmatrix} \sigma_x(\varepsilon_x - \alpha T) + \sigma_y(\varepsilon_y - \alpha T) \\ +\tau_{xy}\gamma_{xy} + \tau_{yz}\gamma_{yz} + \tau_{xz}\gamma_{xz} \end{bmatrix} dxdydz \tag{21}$$

For the current case, the virtual work principle can be stated as follows

$$\int\int \begin{bmatrix} N_x\delta\varepsilon_x^0 + N_y\delta\varepsilon_y^0 + N_{xy}\delta\gamma_{xy}^0 + M_x^b\delta k_x^b \\ +M_y^b\delta k_y^b + M_{xy}^b\delta k_{xy}^b + M_x^s\delta k_x^s + M_y^s\delta k_y^s \\ +M_{xy}^s\delta k_{xy}^s + S_{yz}^s\delta\gamma_{yz}^s + S_{xz}^s\delta\gamma_{xz}^s \end{bmatrix} dxdy = 0 \tag{22}$$

where

$$\begin{Bmatrix} N_x & N_y & N_{xy} \\ M_x^b & M_y^b & M_{xy}^b \\ M_x^s & M_y^s & M_{xy}^s \end{Bmatrix} = \int_{-h/2}^{h/2} (\sigma_x, \sigma_y, \tau_{xy}) \begin{Bmatrix} 1 \\ z \\ f(z) \end{Bmatrix} dz, \tag{23a}$$

$$(S_{xz}^s, S_{yz}^s) = \int_{-h/2}^{h/2} (\tau_{xz}, \tau_{yz}) g(z) dz \tag{23b}$$

Using Eq. (19) in Eq. (23), the stress resultants of the FG plate can be related to the total strains by

$$\begin{Bmatrix} N \\ M^b \\ M^s \end{Bmatrix} = \begin{bmatrix} A & B & B^s \\ B & D & D^s \\ B^s & D^s & H^s \end{bmatrix} \begin{Bmatrix} \varepsilon \\ k^b \\ k^s \end{Bmatrix} - \begin{Bmatrix} N^T \\ M^{bT} \\ M^{sT} \end{Bmatrix}, \; S = A^s\gamma \tag{24}$$

where

$$N = \{N_x, N_y, N_{xy}\}^t, M^b = \{M_x^b, M_y^b, M_{xy}^b\}^t, M^s = \{M_x^s, M_y^s, M_{xy}^s\}^t, \tag{25a}$$

$$N^T = \{N_x^T, N_y^T, 0\}^t, M^{bT} = \{M_x^{bT}, M_y^{bT}, 0\}^t, M^{sT} = \{M_x^{sT}, M_y^{sT}, 0\}^t, \tag{25b}$$

$$\varepsilon = \{\varepsilon_x^0, \varepsilon_y^0, \gamma_{xy}^0\}, \; k^b = \{k_x^b, k_y^b, k_{xy}^b\}, k^s = \{k_x^s, k_y^s, k_{xy}^s\}, \tag{25c}$$

$$A=\begin{bmatrix}A_{11} & A_{12} & 0\\ A_{12} & A_{22} & 0\\ 0 & 0 & A_{66}\end{bmatrix},B=\begin{bmatrix}B_{11} & B_{12} & 0\\ B_{12} & B_{22} & 0\\ 0 & 0 & B_{66}\end{bmatrix},D=\begin{bmatrix}D_{11} & D_{12} & 0\\ D_{12} & D_{22} & 0\\ 0 & 0 & D_{66}\end{bmatrix} \tag{25d}$$

$$B^s=\begin{bmatrix}B^s_{11} & B^s_{12} & 0\\ B^s_{12} & B^s_{22} & 0\\ 0 & 0 & B^s_{66}\end{bmatrix},D^s=\begin{bmatrix}D^s_{11} & D^s_{12} & 0\\ D^s_{12} & D^s_{22} & 0\\ 0 & 0 & D^s_{66}\end{bmatrix},H^s=\begin{bmatrix}H^s_{11} & H^s_{12} & 0\\ H^s_{12} & H^s_{22} & 0\\ 0 & 0 & H^s_{66}\end{bmatrix} \tag{25e}$$

where A_{ij}, B_{ij}, etc., are the plate stiffness, defined by

$$\begin{Bmatrix}A_{11} & B_{11} & D_{11} & B^s_{11} & D^s_{11} & H^s_{11}\\ A_{12} & B_{12} & D_{12} & B^s_{12} & D^s_{12} & H^s_{12}\\ A_{66} & B_{66} & D_{66} & B^s_{66} & D^s_{66} & H^s_{66}\end{Bmatrix}=\int_{-h/2}^{h/2} C_{11}(1,z,z^2,f(z),z\,f(z),f^2(z))\begin{Bmatrix}1\\ \nu\\ \dfrac{1-\nu}{2}\end{Bmatrix}dz \tag{26a}$$

and

$$(A_{22},B_{22},D_{22},B^s_{22},D^s_{22},H^s_{22})=(A_{11},B_{11},D_{11},B^s_{11},D^s_{11},H^s_{11}) \tag{26b}$$

$$A^s_{44}=A^s_{55}=\int_{-h/2}^{h/2}\frac{E(z)}{2(1+\nu)}[g(z)]^2dz, \tag{26c}$$

For thermal loading the stress and moment resultants, $N^T_x=N^T_y$, $M^{bT}_x=M^{bT}_y$, and $M^{sT}_x=M^{sT}_y$ can be written as:

$$\begin{Bmatrix}N^T_x\\ M^{bT}_x\\ M^{bT}_s\end{Bmatrix}=\int_{-h/2}^{h/2}\frac{E(z)}{(1-\nu)}\alpha(z)T\begin{Bmatrix}N^T\\ M^{bT}\\ M^{sT}\end{Bmatrix} \tag{27}$$

The equilibrium criterion can be used to obtain the plate's stability equations. Presume that the displacement components $(u^0_0,v^0_0,w^0_b,w^0_s)$ define the equilibrium condition of the FG plate under thermal stress. An adjacent stable state's displacement components $(u^1_0,v^1_0,w^1_b,w^1_s)$ vary by in relation to the equilibrium position. Accordingly, a nearby state's total displacements are [26].

$$u_0=u^0_0+u^1_0,\ v_0=v^0_0+v^1_0,\ w_b=w^0_b+w^1_b,\ w_s=w^0_s+w^1_s \tag{28}$$

where the state of equilibrium circumstances is denoted by superscript 0 and the state of stability by superscript 1.

Through the substitution of Eqs. (17, 28) into Eq. (22) and subsequent integration by parts, and then equating the coefficients of $\delta u^1_0,\delta v^1_0,\delta w^1_b$ and δw^1_s, the governing stability equations for the shear deformation plate theories can be obtained as follows:

$$\begin{aligned}
&\delta\,u_0\colon\ \frac{\partial N^1_x}{\partial x}+\frac{\partial N^1_{xy}}{\partial y}=0\\
&\delta\,v_0\colon\ \frac{\partial N^1_{xy}}{\partial x}+\frac{\partial N^1_y}{\partial y}=0\\
&\delta\,w_b\colon\ \frac{\partial^2 M^{b1}_x}{\partial x^2}+2\frac{\partial^2 M^{b1}_{xy}}{\partial x\partial y}+\frac{\partial^2 M^{b1}_y}{\partial y^2}+\overline{N}=0
\end{aligned} \tag{29}$$

$$\delta w_s: \quad \frac{\partial^2 M_x^{s1}}{\partial x^2} + 2\frac{\partial^2 M_{xy}^{s1}}{\partial x \partial y} + \frac{\partial^2 M_y^{s1}}{\partial y^2} + \frac{\partial S_{xz}^{s1}}{\partial x} + \frac{\partial S_{yz}^{s1}}{\partial y} + \overline{N} = 0$$

with

$$\overline{N} = \left[N_x^0 \frac{\partial^2 \left(w_b^1 + w_s^1\right)}{\partial x^2} + N_y^0 \frac{\partial^2 \left(w_b^1 + w_s^1\right)}{\partial y^2} \right] \tag{30}$$

where the terms N_x^0 and N_y^0 are the pre-buckling force resultants obtained as

$$N_x^0 = N_y^0 = -\int_{-h/2}^{h/2} \frac{\alpha(z)E(z)T}{(1-\nu)} dz \tag{31}$$

It is possible to construct the stability equations in terms of the displacement components by changing Eq. (29), to equal (27). Four stability equations are obtained, which are derived from the current improved shear deformation theory for FG plates [33].

$$A_{11}\frac{\partial^2 u_0^1}{\partial x^2} + A_{66}\frac{\partial^2 u_0^1}{\partial y^2} + (A_{12}+A_{66})\frac{\partial^2 v_0^1}{\partial x \partial y} - B_{11}\frac{\partial^3 w_b^1}{\partial x^3} - (B_{12}+2B_{66})\frac{\partial^3 w_b^1}{\partial x \partial y^2} - B_{11}^s\frac{\partial^3 w_s^1}{\partial x^3} - (B_{12}^s+2B_{66}^s)\frac{\partial^3 w_s^1}{\partial x \partial y^2} = 0 \tag{32a}$$

$$(A_{12}+A_{66})\frac{\partial^2 u_0^1}{\partial x \partial y} + A_{66}\frac{\partial^2 v_0^1}{\partial x^2} + A_{22}\frac{\partial^2 v_0^1}{\partial y^2} - (B_{12}+2B_{66})\frac{\partial^3 w_b^1}{\partial x^2 \partial y} - B_{22}\frac{\partial^3 w_b^1}{\partial y^3} - B_{22}^s\frac{\partial^3 w_s^1}{\partial y^3} - (B_{12}^s+2B_{66}^s)\frac{\partial^3 w_s^1}{\partial x^2 \partial y} = 0 \tag{32b}$$

$$B_{11}\frac{\partial^3 u_0^1}{\partial x^3} + (B_{12}+2B_{66})\frac{\partial^3 u_0^1}{\partial x \partial y^2} + (B_{12}+2B_{66})\frac{\partial^3 v_0^1}{\partial x^2 \partial y} + B_{22}\frac{\partial^3 v_0^1}{\partial y^3} - D_{11}\frac{\partial^4 w_b^1}{\partial x^4} - 2(D_{12}+2D_{66})\frac{\partial^4 w_b^1}{\partial x^2 \partial y^2} - D_{22}\frac{\partial^4 w_b^1}{\partial y^4} - D_{11}^s\frac{\partial^4 w_s^1}{\partial x^4} - 2(D_{12}^s+2D_{66}^s)\frac{\partial^4 w_s^1}{\partial x^2 \partial y^2} - D_{22}^s\frac{\partial^4 w_s^1}{\partial y^4} + \overline{N} = 0 \tag{32c}$$

$$B_{11}^s\frac{\partial^3 u_0^1}{\partial x^3} + (B_{12}^s+2B_{66}^s)\frac{\partial^3 u_0^1}{\partial x \partial y^2} + (B_{12}^s+2B_{66}^s)\frac{\partial^3 v_0^1}{\partial x^2 \partial y} + B_{22}^s\frac{\partial^3 v_0^1}{\partial y^3} - D_{11}^s\frac{\partial^4 w_b^1}{\partial x^4} - 2(D_{12}^s+2D_{66}^s)\frac{\partial^4 w_b^1}{\partial x^2 \partial y^2} - D_{22}^s\frac{\partial^4 w_b^1}{\partial y^4} - H_{11}^s\frac{\partial^4 w_s^1}{\partial x^4} - 2(H_{12}^s+2H_{66}^s)\frac{\partial^4 w_s^1}{\partial x^2 \partial y^2} - H_{22}^s\frac{\partial^4 w_s^1}{\partial y^4} + A_{55}^s\frac{\partial^2 w_s^1}{\partial x^2} + A_{44}^s\frac{\partial^2 w_s^1}{\partial y^2} + \overline{N} = 0 \tag{32d}$$

2.6 Trigonometric solution of thermal buckling

Rectangular plates are often categorized based on the kind of support that is utilized. The analytical solutions of Eq. (32) for a simply supported porous FG plate are what we are interested in here. At the side edges, the following boundary restrictions are in place.

$$v_0^1 = w_b^1 = w_s^1 = \frac{\partial w_s^1}{\partial y} = N_x^1 = M_x^{b1} = M_x^{s1} = 0 \text{at } x = 0, a \tag{33a}$$

$$u_0^1 = w_b^1 = w_s^1 = \frac{\partial w_s^1}{\partial x} = N_y^1 = M_y^{b1} = M_x^{s1} = 0 \text{at } y = 0, b \tag{33b}$$

The following approximate solution is seen to satisfy both the differential equation and the boundary conditions

$$\begin{Bmatrix} u_0^1 \\ v_0^1 \\ w_b^1 \\ w_s^1 \end{Bmatrix} = \sum_{m=1}^{\infty}\sum_{n=1}^{\infty} \begin{Bmatrix} U_{mn}^1 \cos(\lambda x)\sin(\mu y) \\ V_{mn}^1 \sin(\lambda x)\cos(\mu y) \\ W_{bmn}^1 \sin(\lambda x)\sin(\mu y) \\ W_{smn}^1 \sin(\lambda x)\sin(\mu y) \end{Bmatrix} \tag{34}$$

where U_{mn}^1; V_{mn}^1; W_{bmn}^1; and W_{smn}^1 are arbitrary parameters to be determined, $\lambda = m\pi/a$ and $\mu = n\pi/b$and m and n are mode numbers. Substituting Eq. (34) into Eq. (32), one obtains

$$[K]\{\Delta\} = \{0\} \tag{35}$$

where $\{\Delta\}$ denotes the column

$$\{\Delta\}^T = \{U_{mn}^1, V_{mn}^1, W_{bmn}^1, W_{smn}^1\} \tag{36}$$

and $[K]$ is the symmetric matrix given by

$$[K] = \begin{bmatrix} s_{11} & s_{12} & s_{13} & s_{14} \\ s_{12} & s_{22} & s_{23} & s_{24} \\ s_{13} & s_{23} & s_{33} & s_{34} \\ s_{14} & s_{24} & s_{34} & s_{44} \end{bmatrix} \tag{37}$$

in which:

$$\begin{gathered} s_{11} = -(A_{11}\lambda^2 + A_{66}\mu^2) \\ s_{12} = -\lambda\,\mu\,(A_{12} + A_{66}) \\ s_{13} = -\lambda\,[B_{11}\lambda^2 + (B_{12} + 2B_{66})\,\mu^2] \\ s_{14} = \lambda\,[B_{11}^s\lambda^2 + (B_{12}^s + 2B_{66}^s)\,\mu^2] \\ s_{22} = -(A_{66}\lambda^2 + A_{22}\mu^2) \\ s_{23} = \mu\,[(B_{12} + 2B_{66})\,\lambda^2 + B_{22}\mu^2] \\ s_{24} = \mu\,[(B_{12}^s + 2B_{66}^s)\,\lambda^2 + B_{22}^s\mu^2] \\ s_{33} = -\left(D_{11}\lambda^4 + 2(D_{12} + 2D_{66})\lambda^2\mu^2 + D_{22}\mu^4 + N_x^0\lambda^2 + N_y^0\mu^2\right) \\ s_{34} = -\left(D_{11}^s\lambda^4 + 2(D_{12}^s + 2D_{66}^s)\lambda^2\,\mu^2 + D_{22}^s\,\mu^4 + N_x^0\lambda^2 + N_y^0\mu^2\right) \\ s_{44} = -\left(H_{11}^s\lambda^4 + 2(H_{12}^s + 2H_{66}^s)\lambda^2\mu^2 + H_{22}^s\mu^4 + A_{55}^s\lambda^2 + A_{44}^s\mu^2 + N_x^0\lambda^2 + N_y^0\mu^2\right) \end{gathered} \tag{38}$$

2.7 Buckling of FG plates under uniform temperature rise

It is assumed that the plate initial temperature is T_i. The temperature is uniformly raised to a final value T_f in which the plate buckles. The temperature change is $\Delta T = T_f - T_i$. The thermal force resultant and is evaluated as

Table 1. Material properties used in the FG plate

Properties	Ceramic	Metal
	Al_2O_3	Al
$E(GPa)$	380	70
$\alpha(/^{\circ}C)$	$7.4.10^{-6}$	23.10^{-6}

$$N_{cr} = -\int_{-h/2}^{h/2} \frac{\alpha(z)E(z)\left(T_f - T_i\right)}{(1-\nu)} dz \tag{39}$$

By solving the determinant of Eq. (37) one can easily obtain the critical buckling temperature change t_{cr}.

2.8 Buckling of FG plates subjected to graded temperature change across the thickness

The plate top surface temperature is T_M while the bottom surface temperature is T_b. Further, the temperature along the thickness varies as per power law and is given by:

$$T(z) = \Delta T \left(\frac{z}{h} + \frac{1}{2}\right)^{\gamma_1} + T_M \tag{40}$$

where the buckling temperature difference $\Delta T = T_C - T_M$ and γ_1 is the temperature exponent $(0 \prec \gamma_1 \prec \infty)$. It is to be noted that when the parameter γ_1 is unity it shows a linear change in temperature. Also, γ_1 is greater than unity shows a non-linear temperature change. Likewise, the critical buckling temperature change t_{cr} can be attained.

3. Numerical results numerical results and discussion

The thermal buckling of simply supported imperfect FG plates under uniform, linear, and nonlinear thermal loading over the thickness is described numerically in this section. The results obtained are compared with those obtained by Javaheri and Eslami [34], and Zenkour and Mashat [26] for verification formulations.

The functionally graded plate is thought to be composed of an alumina and aluminum alloy. Table 1 lists the aluminum and alumina's Young modulus, and coefficient of thermal expansion.

Table 2 shows the validation of the present study with the theoretical models HPT, CPT, and SPT, where CPT values are generally slightly higher than HPT and SPT values, indicating a minor variation in the predicted buckling loads. The maximum buckling temperature was obtained for type 1 followed by type 6, type 4, type 2, type 3 and type 5.

Table 3 presents the results for a functionally graded square plate under uniform temperature rise, considering various indices (*k*) and side-to-thickness ratios (*a/h*). The buckling loads for different types and theories at various *a/h* values are reported for *k* values of 0, 1, 5, and 10. Across all porosity types, from type 1 to type 6, the buckling load consistently decreases as the *a/h* ratio increases. This trend is consistent for all values of *k*, indicating that as the aspect ratio increases, structural stability decreases, which is reflected in the reduced buckling loads. A significant reduction in buckling load nearly 100% was observed as the *a/h* ratio increased from 10 to 100.

Table 2. Buckling temperature calculation at uniform temperature rise for different values of power law index k and aspect ratio *a/b* with *a/h* = 100 and β = 0.1

k	Theory		*a/b*=1	*a/b*=2	*a/b*=3	*a/b*=4	*a/b*=5
0	Present	Type 1	17.09	42.69	85 .26	144.65	220.67
		Type 2	17.09	42.69	85 .26	144.65	220.67
		Type 3	17.09	42.69	85 .26	144.65	220.67
		Type 4	17.09	42.69	85 .26	144.65	220.67
		Type 5	17.09	42.69	85 .26	144.65	220.67
		Type 6	17.09	42.69	85 .26	144.65	220.67
	HPT [34]		17.08	42.68	85.25	144.64	220.66
	SPT [26]		17.08	42.68	85.25	144.65	220.67
	CPT [34]		17.09	42.74	85.49	145.34	222.28
1	Present	Type 1	7.94	19.84	39.62	67.25	102.64
		Type 2	7.70	19.24	38.45	65.27	99.61
		Type 3	7.66	19.15	38.25	64.92	99.10
		Type 4	7.74	19.34	38.64	65.59	100.11
		Type 5	7.60	18.98	37.92	64.37	98.25
		Type 6	7.80	19.48	38.91	66.04	100.80
	HPT [34]		7,94	19.83	39.62	67.25	102.63
	SPT [26]		7,94	19.83	39.62	67.25	102.63
	CPT [34]		7,94	19.85	39.71	67.52	103.26
5	Present	Type 1	7.26	18.13	36.20	61.40	93.61
		Type 2	6.98	17.44	34.82	59.06	90.05
		Type 3	6.91	17.26	34.47	58.46	89.13
		Type 4	7.04	17.59	35.13	59.57	90.83
		Type 5	6.78	16.93	33.81	57.35	87.44
		Type 6	7.12	17.78	35.50	60.20	91.79
	HPT [34]		7.26	18.13	36.20	61.39	93.60
	SPT [26]		7.26	18.13	36.20	61.39	93.60
	CPT [34]		7.26	18.16	36.32	61.75	94.45
10	Present	Type 1	7.46	18.64	37.20	63.07	96.12
		Type 2	7.56	18.89	37.70	63.90	97.37
		Type 3	7.56	18.88	37.68	63.87	97.32
		Type 4	7.56	18.88	37.68	37.68	97.33
		Type 5	7.54	18.83	37.58	63.69	97.04
		Type 6	7.55	18.84	37.61	63.76	97.16
	HPT [34]		7.46	18.63	37.20	63.06	96.12
	SPT [26]		7.46	18.63	37.20	63.06	96.11
	CPT [34]		7.46	18.67	37.34	63.48	97.10

Table 3. Buckling temperature calculation at uniform temperature rise for different values of power law index k and side-to-thickness ratio a/h and β = 0.1

k	Theory		*a/h*=10	*a/h*=20	*a/h*=40	*a/h*=60	*a/h*=80	*a/h*=100
0	Present	Type 1	1618.68	421.54	106.49	47.42	26.69	17.08
		Type 2	1618.68	421.54	106.49	47.42	26.69	17.08
		Type 3	1618.68	421.54	106.49	47.42	26.69	17.08
		Type 4	1618.68	421.54	106.49	47.42	26.69	17.08
		Type 5	1618.68	421.54	106.49	47.42	26.69	17.08
		Type 6	1618.68	421.54	106.49	47.42	26.69	17.08
	HPT [34]		1617.48	1617.48	421.52	106.49	47.42	17.08
	CPT [34]		1709.91	1709.91	427.47	106.87	47.49	17.09
1	Present	Type 1	758.39	196.27	49.50	22.04	12.40	7.94
		Type 2	737.36	190.54	48.04	21.38	12.04	7.70
		Type 3	733.71	189.55	47.79	21.27	11.97	7.66
		Type 4	740.80	191.47	48.28	21.49	12.10	7.74
		Type 5	727.82	187.95	47.38	21.09	11.87	7.60
		Type 6	745.60	192.78	48.61	21.64	12.18	7.80
	HPT [34]		757,89	196,26	49,50	22,03	12,40	7,94
	CPT [34]		794,37	198,59	49,64	22,06	12,41	7,94
5	Present	Type 1	679.31	178.54	45.21	20.14	11.34	7.26
		Type 2	654.29	171.79	43.49	19.38	10.91	6.98
		Type 3	647.88	170.04	43.05	19.18	10.80	6.91
		Type 4	659.74	173.26	43.87	19.54	11.00	7.04
		Type 5	636.07	166.84	42.23	18.81	10.59	6.78
		Type 6	666.43	175.07	44.33	19.75	11.12	7.12
	HPT [34]		678.92	178.53	45.21	20.14	11.34	7.26
	CPT [34]		726.57	181.64	45.41	20.18	11.35	7.26
10	Present	Type 1	692.69	183.14	46.46	20.70	11.65	7.46
		Type 2	699.11	185.41	47.07	20.98	11.81	7.56
		Type 3	698.39	185.32	47.05	20.97	11.81	7.56
		Type 4	699.23	185.36	47.05	20.97	11.81	7.56
		Type 5	695.78	184.76	46.92	20.91	11.78	7.54
		Type 6	698.57	185.06	46.97	20.93	11.79	7.55
	HPT [34]		692.52	183.14	46.45	20.70	11.65	7.46
	CPT [34]		746.92	186.73	46.68	20.74	11.67	7.46

Table 4 illustrates the change in buckling temperature under linear temperature variation for different thicknesses and indices. The trend in buckling temperature variation was found to be similar to that of uniform temperature analysis, though its magnitude is comparatively higher. As the parameter *a/b* increases from 1 to 5, the magnitude increases significantly. The theoretical

Table 4. Buckling temperature calculation at linear temperature rise for different k and *a/b* while *a/h* =100 and β = 0.1

k	Theory		*a/b*=1	*a/b*=2	*a/b*=3	*a/b*=4	*a/b*=5
0	Present	Type 1	75.37	160.51	279.29	431.34	220.67
		Type 2	75.37	160.51	279.29	431.34	220.67
		Type 3	75.37	160.51	279.29	431.34	220.67
		Type 4	75.37	160.51	279.29	431.34	220.67
		Type 5	75.37	160.51	279.29	431.34	220.67
		Type 6	75.37	160.51	279.29	431.34	220.67
	HPT [34]		24.17	75.37	160.50	279.29	431.33
	SPT [26]		24.17	75.37	160.51	279.30	431.34
	CPT [34]		24.19	75.49	160.99	280.68	434.57
1	Present	Type 1	27.82	64.93	116.74	183.11	102.64
		Type 2	25.98	61.00	109.89	172.53	99.61
		Type 3	25.68	60.37	108.79	170.84	99.10
		Type 4	26.26	61.61	110.95	174.17	100.11
		Type 5	25.21	59.37	107.06	168.16	98.25
		Type 6	26.67	62.48	112.47	176.50	100.80
	HPT [34]		5.51	27.82	64.93	116.74	183.11
	SPT [26]		5.51	27.82	64.93	116.74	183.11
	CPT [34]		5.52	27.86	65.11	117.25	184.30
5	Present	Type 1	22.60	53.70	97.07	152.51	93.61
		Type 2	20.23	48.51	87.93	138.35	90.05
		Type 3	19.75	47.46	86.09	135.50	89.13
		Type 4	20.67	49.46	89.59	140.92	90.83
		Type 5	18.91	45.65	82.95	130.65	87.44
		Type 6	21.25	50.72	91.80	144.34	91.79
	HPT [34]		3.89	22.60	53.71	97.07	152.51
	SPT [26]		3.89	22.60	53.70	97.06	152.50
	CPT [34]		3.89	22.65	53.92	97.69	153.97
10	Present	Type 1	24.16	57.06	102.90	161.47	96.12
		Type 2	23.33	54.93	98.96	155.19	97.37
		Type 3	23.08	54.36	97.93	153.57	97.32
		Type 4	23.53	55.41	99.82	156.55	97.33
		Type 5	22.62	53.29	96.01	150.58	97.04
		Type 6	23.76	55.98	100.88	158.22	97.16
	HPT [34]		4.36	24.16	57.06	102.90	161.47
	SPT [26]		4.36	24.16	57.06	102.89	161.46
	CPT [34]		4.37	24.23	57.32	103.64	163.20

Table 5. Buckling temperature calculation at linear temperature rise for different k, *a/h* and β = 0.1

k	Theory		*a/h*=10	*a/h*=20	*a/h*=40	*a/h*=60	*a/h*=80	*a/h*=100
0	Present	Type 1	3227.36	833.07	202.98	84.84	43.38	24.17
		Type 2	3227.36	833.07	202.98	84.84	43.38	24.17
		Type 3	3227.36	833.07	202.98	84.84	43.38	24.17
		Type 4	3227.36	833.07	202.98	84.84	43.38	24.17
		Type 5	3227.36	833.07	202.98	84.84	43.38	24.17
		Type 6	3227.36	833.07	202.98	84.84	43.38	24.17
	HPT [34]		3224,96	833,03	202,98	84,84	43,38	24,17
	CPT [34]		3409,82	844,95	203,73	84,99	43,43	24,19
1	Present	Type 1	1412.96	358.71	83.46	31.95	13.88	5.51
		Type 2	1335.49	338.340	78.48	29.87	12.82	4.93
		Type 3	1323.05	335.06	77.68	29.54	12.65	4.83
		Type 4	1347.46	341.48	79.25	30.19	12.99	5.02
		Type 5	1303.43	329.91	76.42	29.01	12.38	4.68
		Type 6	1364.57	345.98	80.35	30.65	13.22	1.36
	HPT [34]		1412.02	358.69	83.46	31.95	13.88	5.51
	CPT [34]		1480.45	363.07	83.73	32.00	13.90	5.52
5	Present	Type 1	1160.68	298.70	69.21	26.06	10.91	3.89
		Type 2	1056.17	271.30	62.61	23.38	9.61	3.22
		Type 3	1035.42	265.82	61.28	22.83	9.33	3.07
		Type 4	1074.99	276.26	63.81	23.87	9.85	3.35
		Type 5	1000.10	256.47	58.99	21.88	8.85	2.82
		Type 6	1100.09	282.86	65.41	24.53	10.17	3.52
	HPT [34]		1160.02	298.69	69.21	26.06	10.91	3.89
	CPT [34]		1242.03	304.05	69.55	26.13	10.93	3.89
10	Present	Type 1	1218.63	315.68	73.46	27.82	11.79	4.36
		Type 2	1166.23	303.13	70.68	26.85	11.44	4.30
		Type 3	1153.47	299.96	69.95	26.57	11.32	4.26
		Type 4	1177.18	305.83	71.30	27.08	11.54	4.34
		Type 5	1130.14	294.09	68.58	26.03	11.08	4.15
		Type 6	1190.80	309.14	72.05	27.35	11.65	4.37
	HPT [34]		1218.32	315.67	73.46	27.82	11.79	4.36
	CPT [34]		1314.74	322.04	73.86	27.90	11.82	4.37

models used for validation, HPT, SPT, and CPT follow the same increasing trend with slight variations. Notably, CPT values are generally slightly higher than those of HPT and SPT.

Tables 6, 7 analyze the critical buckling temperature under a non-linear temperature rise for different *a/h* values, specifically 5 and 10. These tables show that the plate experiences a lower

Table 6. Buckling temperature calculation at non-linear temperature rise for different k and *a/b* temperature exponent γ_1 with *a/h* = 10

k	Theory		*a/b*=1			*a/b*=2			*a/b*=3		
			γ_1=2	γ_1=5	γ_1=10	γ_1=2	γ_1=5	γ_1=10	γ_1=2	γ_1=5	γ_1=10
0	Present	Type 1	4.84	9.68	17.75	11.22	22.45	41.17	20.01	40.01	73.36
		Type 2	4.84	9.68	17.75	11.22	22.45	41.17	20.01	40.01	73.36
		Type 3	4.84	9.68	17.75	11.22	22.45	41.17	20.01	40.01	73.36
		Type 4	4.84	9.68	17.75	11.22	22.45	41.17	20.01	40.01	73.36
		Type 5	4.84	9.68	17.75	11.22	22.45	41.17	20.01	40.01	73.36
		Type 6	4.84	9.68	17.75	11.22	22.45	41.17	20.01	40.01	73.36
	HPT [34]		4,84	9,68	17,75	11,22	22,45	41,16	20,00	40,01	73,35
	SPT [26]		4,84	9,68	17,75	11,22	22,45	41,17	20,01	40,03	73,39
	CPT [34]		5,11	10,22	18,75	12,80	25,61	46,96	25,63	51,26	93,99
1	Present	Type 1	2.11	4.32	8.19	4.95	10.15	19.25	8.97	18.38	34.86
		Type 2	1.97	4,00	7.54	4.64	9.42	17.78	8.44	17.12	32.32
		Type 3	1.95	3.95	7.44	4.60	9.30	17.55	8.36	16.93	31.93
		Type 4	1.99	4.04	7.64	4.69	9.53	18,00	8.52	17.31	32.70
		Type 5	1.92	3.87	7.29	4.52	9.13	17.20	8.23	16.62	31.32
		Type 6	2.02	4.11	7.78	4.76	9.69	18.31	8.64	17.58	33.25
	HPT [34]		2,1066	4,31	8,19	4,95	10,14	19,24	8,96	18,38	34,86
	SPT [26]		2,1068	4,31	8,19	9,95	10,14	19,25	8,97	18,38	34,87
	CPT [34]		2,20	4,52	8,58	5,53	11,35	21,53	11,09	22,73	43,12
5	Present	Type 1	1.60	2.85	5.00	3.65	6.52	11.44	6.38	11.38	19.98
		Type 2	1.41	2.42	4.16	3.23	5.55	9.53	5.66	9.71	16.67
		Type 3	1.38	2.35	4.02	3.16	5.38	9.21	5.53	9.43	16.13
		Type 4	1.44	2.49	4.29	3.30	5.71	9.83	5.78	9.98	17.19
		Type 5	1.32	2.23	3.79	3.03	5.11	8.70	5.31	8.97	15.27
		Type 6	1.49	2.59	4.48	3.40	5.93	10.26	5.94	10.36	17.92
	HPT [34]		1.59	2.85	5.00	3.65	6.52	11.44	6.37	11.38	19.97
	SPT [26]		1.59	2.84	4.99	3.64	6.51	11.43	6.36	11.36	19.93
	CPT [34]		1.70	3.04	5.35	4.28	7.65	13.43	8.58	15.33	26.90
10	Present	Type 1	1.68	2.89	4.77	3.80	6.53	10.81	6.54	11.25	18.61
		Type 2	1.55	2.53	4.05	3.50	5.71	9.11	5.98	9.76	15.59
		Type 3	1.53	2.47	3.92	3.43	5.56	8.82	5.87	9.49	15.08
		Type 4	1.58	2.59	4.16	3.55	5.84	9.39	6.08	10.01	16.07
		Type 5	1.48	2.36	3.72	3.32	5.31	8.35	5.68	9.06	14.26
		Type 6	1.61	2.67	4.33	3.62	6.04	9.77	6.22	10.35	16.75
	HPT [34]		1,67	2,88	4,77	3,79	6,53	10,80	6,54	11,25	18,61
	SPT [26]		1,67	2,88	4,77	3,79	6,53	10,80	6,53	11,24	18,60
	CPT [34]		1,80	3,11	5,14	4,54	7,81	12,92	9,09	15,64	25,88

Table 7. Buckling temperature calculation at linear temperature rise for different k, *a/b* and temperature exponent γ_1 with *a/h* = 5

k	Theory		*a/b*=1			*a/b*=2			*a/b*=3		
			γ_1=2	γ_1=5	γ_1=10	γ_1=2	γ_1=5	γ_1=10	γ_1=2	γ_1=5	γ_1=10
0	Present	Type1	16.74	33.47	61.36	32.86	65.73	120.50	48.54	97.08	177.98
		Type2	16.74	33.47	61.36	32.86	65.73	120.50	48.54	97.08	177.98
		Type3	16.74	33.47	61.36	32.86	65.73	120.50	48.54	97.08	177.98
		Type4	16.74	33.47	61.36	32.86	65.73	120.50	48.54	97.08	177.98
		Type5	16.74	33.47	61.36	32.86	65.73	120.50	48.54	97.08	177.98
		Type6	16.74	33.47	61.36	32.86	65.73	120.50	48.54	97.08	177.98
	HPT [34]		16,73	33,47	61,36	32,86	65,72	120,49	48,53	97,07	177,97
	SPT [26]		16,74	33,48	61,38	32,89	65,79	120,62	48,65	97,30	178,39
	CPT [34]		20,50	41,00	75,18	51,28	102,56	188,03	102,57	205,15	376,12
1	Present	Type1	7.46	15.28	28.99	15.08	30.91	58.63	22.92	46.98	89.11
		Type2	7.01	14.22	26.83	14.28	28.96	54.67	21.87	44.34	83.70
		Type3	6,94	14.05	26.50	14.15	28.66	54.06	21.70	28.94	82.87
		Type4	7.08	14.38	27.16	14.40	29.25	55.26	22.03	44.74	84.51
		Type5	6.83	13.79	25.99	13.96	28.19	53.11	21.44	43.30	81.58
		Type6	7.18	14.61	27.62	14.58	29.68	56.12	22.26	45.31	85.68
	HPT [34]		7.45	15.28	28.98	15.08	30.90	58.62	22.92	46.98	89.11
	SPT [26]		7.45	15.28	28.99	15.09	30.93	58.68	22.97	47.08	89.30
	CPT [34]		8.87	18.18	34.48	22.19	45.49	86.30	44.41	91.02	172.65
5	Present	Type1	5.37	9.59	16.84	10.17	18.15	31.86	14.53	25.93	45.51
		Type2	4.76	8.18	14.04	9.05	15.54	26.68	12.99	22.30	38.27
		Type3	4.65	7.94	13.58	8.85	15.10	25.84	12.72	21.70	37.12
		Type4	4.87	8.41	14.48	9.24	15.96	27.48	13.24	22.87	39.38
		Type5	4.47	7.55	12.85	8.53	14.40	24.51	12.28	20.74	35.30
		Type6	5.01	8.73	15.10	9.50	16.54	28.63	13.59	23.68	40.97
	HPT [34]		5.37	9.59	16.83	10.16	18.15	31.85	14.52	25.93	45.51
	SPT [26]		5.36	9.57	16.81	10.14	18.10	31.77	14.49	25.87	45.40
	CPT [34]		6.86	12.26	21.52	17.18	30.68	53.85	34.39	61.39	107.75
10	Present	Type1	5.54	9.53	15.77	10.24	17.62	29.15	14.35	24.68	40.83
		Type2	5.08	8.29	13.24	9.29	15.16	24.21	12.89	21.04	33.60
		Type3	4.99	8.07	12.81	9.10	14.72	23.38	12.62	20.41	32.42
		Type4	5.16	8.50	13.64	9.45	15.56	24.99	13.14	21.63	34.74
		Type5	4.83	7.70	12.12	8.79	14.02	22.06	12.16	19.39	30.53
		Type6	5.27	8.78	14.21	9.68	16.13	26.10	13.48	22.45	36.34
	HPT [34]		5.54	9.53	15.76	10.24	17.62	29.15	14.34	24.68	40.82
	SPT [26]		5.53	9.52	15.75	10.23	17.61	29.13	14.35	24.69	40.85
	CPT [34]		7.27	12.51	20.70	18.20	31.31	51.80	36.41	62.65	103.64

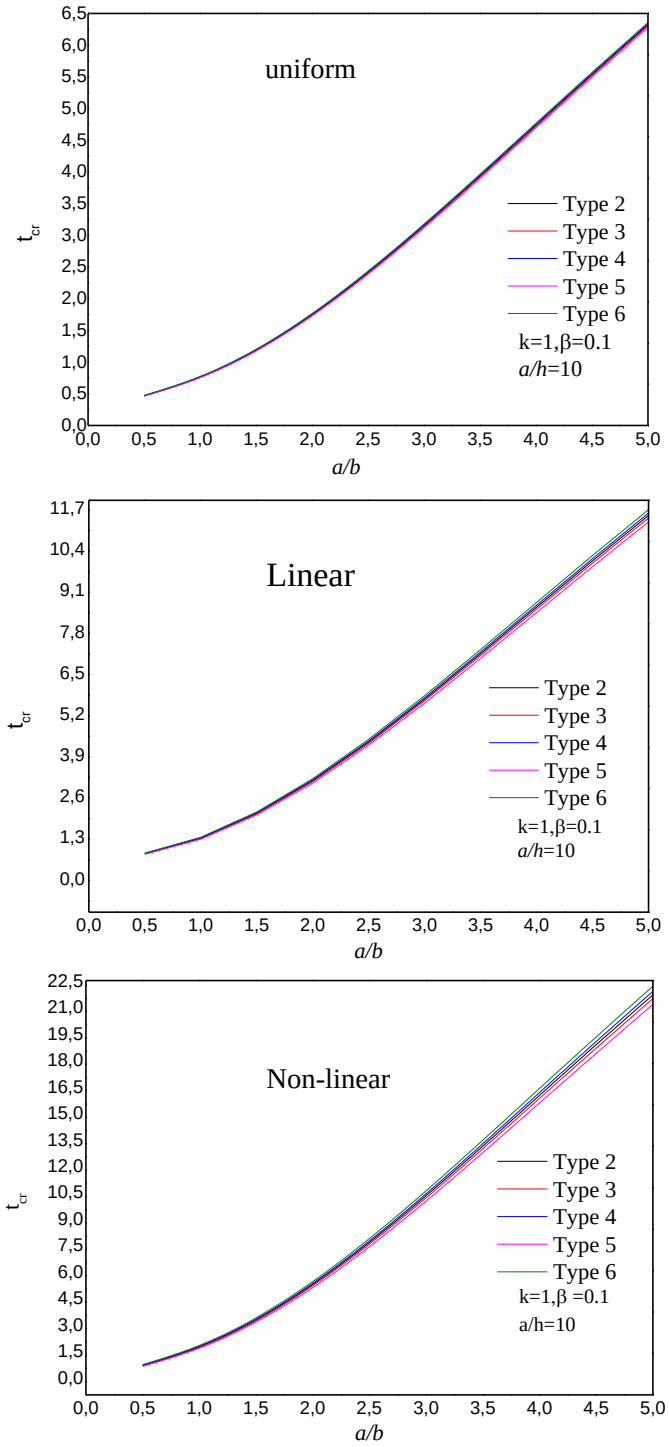

Figure 1. Critical buckling temperature difference t_{cr} due to uniform, linear and non-linear temperature rise across the thickness versus the aspect ratio *a/b* with β = 0.1

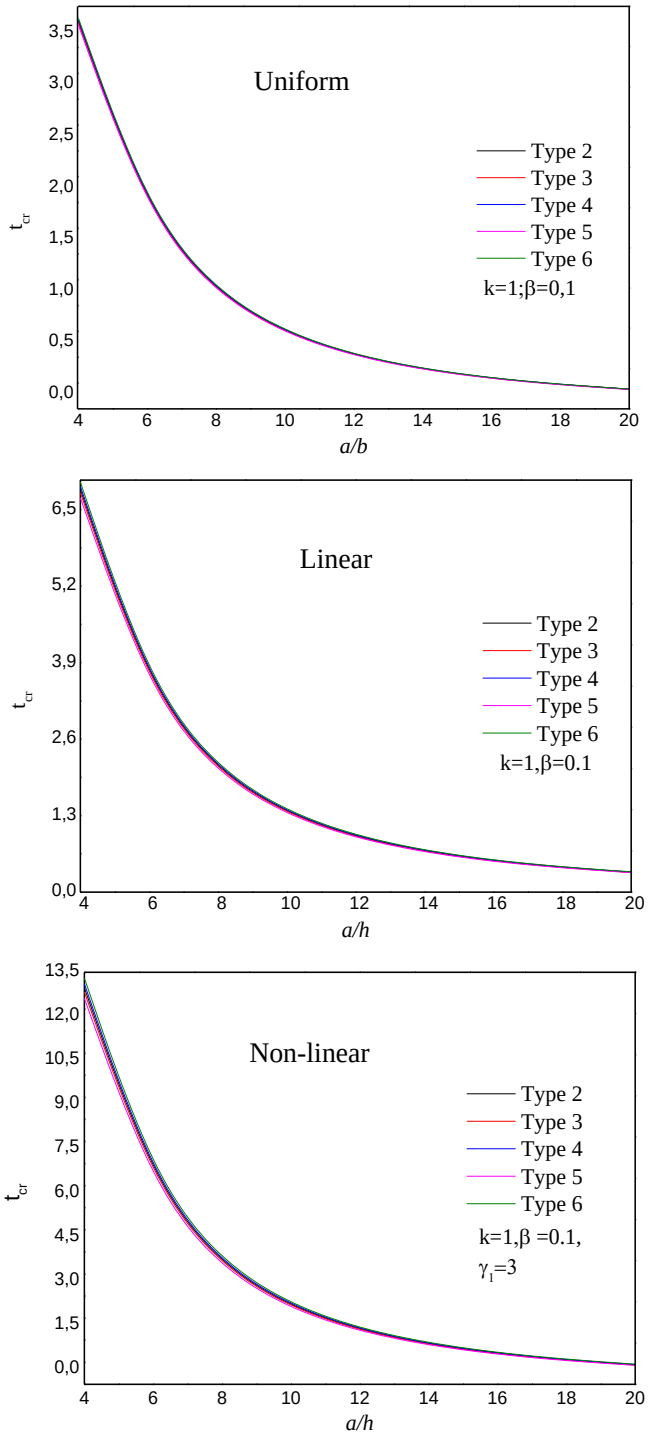

Figure 2. Critical buckling temperature difference t_{cr} due to uniform, linear and non-linear temperature rise across the thickness versus the side-to-thickness ratio *a/h* with $\beta = 0.1$

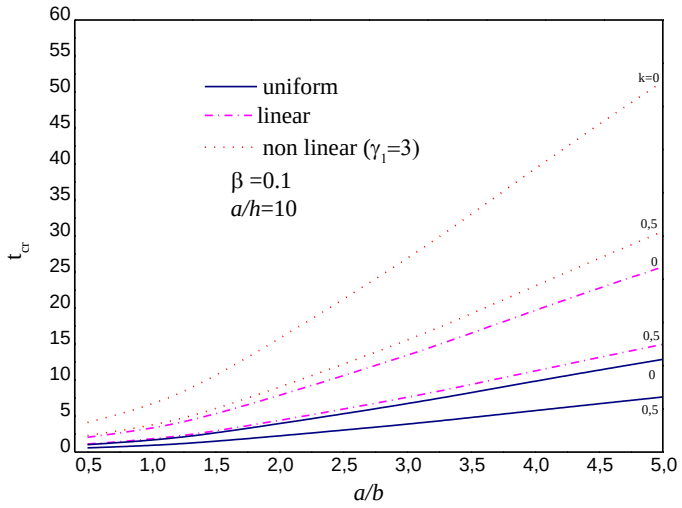

Figure 3. Critical buckling temperature difference t_{cr} due to uniform, linear and non-linear temperature rise across the thickness versus the aspect ratio a/h with β = 0.1 (Type 5)

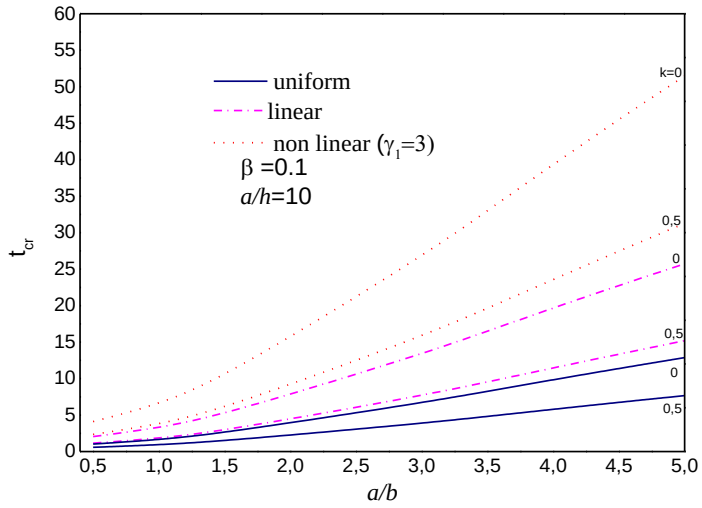

Figure 4. Critical buckling temperature difference t_{cr} due to uniform, linear and non-linear temperature rise across the thickness versus the aspect ratio a/h with β = 0.1 (Type 6)

critical buckling temperature, indicating greater susceptibility to buckling under non-linear temperature variations. This significant reduction in the critical buckling temperature suggests that even minor deviations from a linear temperature profile can lead to structural buckling.

Fig. 1 depicts the frequency variation of a square plate for different side length ratios (*a/b*) with a fixed index value (k=1). Among the various types categorized (Types 2-6), there is no significant variation in magnitude. The greatest change is observed under non-linear temperature variation, followed by linear and uniform temperature variations.

Fig. 2 illustrates the frequency variation of a square plate for different side-to-thickness ratios (*a/h*) and a fixed index value (k=*1*). Similar to the parameter *a/h* impact, here also, among the various types categorized no significant variation in the magnitude was seen between the types of porosity studied.

Fig. 3, 4 show the variation of buckling load for uniform, linear, and non-linear temperature change. It can be seen that for uniform temperature change the buckling load is maximum followed by linear and non-uniform change. It is observed that increasing the parameter *a/b* leads to an increase in frequency. For higher values of *a/b* the buckling load changes to maximum.

4. Conclusions

The trigonometric shear deformation theory was effectively applied to the buckling analysis of FG plates. The following noteworthy findings were observed:

• Varying the *a/b* and *a/h* ratios allowed for the examination of the impact of geometric parameters. Smaller plates exhibit higher stiffness, and it was found that increasing the *a/b* ratio raises the critical buckling temperature (t_{cr}), while an increase in the *a/h* ratio leads to a decrease in buckling temperature. Among these parameters, the buckling load is more significantly affected by the *a/h* ratio than by the *a/b* ratio.

• Under non-linear temperature conditions, the buckling temperature is the lowest, followed by linear and uniform temperature scenarios.

• The buckling load is highest for type 1, followed by type 6, type 4, type 2, type 3, and type 5. This variation is attributed to the fact that as the plate becomes more metal-rich, its critical buckling load increases.

• As the power-law index (*k*) increases, the buckling load decreases. This highlights the critical role of material properties in determining structural behavior. The buckling response is directly influenced by the deformation characteristics of materials with different power-law indices under applied loads.

The effect of porosity was studied by introducing the parameter (β) into the material property variations. A uniform distribution of porosity was assumed, with porosity equally distributed between the metal and ceramic phases.

The results reveal that the critical buckling temperature decreases monotonically with increasing β due to stiffness degradation induced by internal voids. For the FGM system and loading conditions considered, it is observed that the reduction in buckling capacity remains moderate for low-to-intermediate porosity levels, whereas a pronounced decrease occurs beyond a threshold value. Based on the obtained parametric curves and considering conservative design requirements, an admissible range of the porosity parameter may be recommended as $0 \leq \beta \leq 0.2$. Within this interval, the normalized critical buckling temperature remains within acceptable engineering margins compared to the fully dense reference plate, even under nonlinear thermal loading. For β values exceeding this limit, the stability reduction becomes significant, particularly for large a/h ratios and high power-law indices.

Overall, the present analytical results provide practical design guidance for FG porous plates subjected to thermal environments. To ensure safe thermal buckling performance, designers should prioritize adequate thickness (low a/h ratio), consider nonlinear temperature distributions for conservative evaluation, limit the power-law index when high thermal resistance is required, and maintain the porosity parameter within the recommended admissible range.

References

1. Barbaros, I., Yang, Y., Safaei, B., Yang, Z., Qin, Z., Asmael, M. (2022). State-of-the-art review of fabrication, application, and mechanical properties of functionally graded porous nanocomposite materials. Nanotechnology Reviews, 11(1), 321-371. https://doi.org/10.1515/ntrev-2022-0017
2. Madan, R., Bhowmick, S. (2022). Fabrication, microstructural characterization and finite element analysis of functionally graded Al-Al2O3 disk using powder metallurgy technique. Materials Today Communications, 32, 103878. https://doi.org/10.1016/j.mtcomm.2022.103878
3. Madan, R., Bhowmick, S. (2023). Fabrication and microstructural characterization of Al-SiC based functionally graded disk. Aircraft Engineering and Aerospace Technology, 95(2), 292-301. https://doi.org/10.1108/AEAT-03-2022-0096
4. Alibeigloo, A. (2020). Three-dimensional thermoelasticity analysis of graphene platelets reinforced cylindrical panel. European Journal of Mechanics-A/Solids, 81, 103941. https://doi.org/10.1016/j.euromechsol.2019.103941
5. Amirjan, M., Bozorg, M. (2019). Fabrication and properties of Cu-Al2O3 functionally graded nanocomposites prepared by spark plasma sintering: the effect of copper particle size and reinforcement content. Materials Research Express, 6(10), 105011. https://doi.org/10.1088/2053-1591/ab34c5
6. Bykov, Y.V., Egorov, S.V., Eremeev, A.G., Plotnikov, I.V., Rybakov, K.I., Semenov, V.E., ... Holoptsev, V.V. (2012). Fabrication of metal-ceramic functionally graded materials by microwave sintering. Inorganic Materials: Applied Research, 3(3), 261-269. https://doi.org/10.1134/S2075113312030057
7. Kwon, H., Bradbury, C.R., Leparoux, M. (2011). Fabrication of functionally graded carbon nanotube-reinforced aluminum matrix composite. Advanced engineering materials, 13(4), 325-329. https://doi.org/10.1002/adem.201000251
8. Apalak, M.K., Demirbas, M.D. (2015). Thermal residual stresses in in-plane functionally graded clamped hollow circular plates subjected to an edge heat flux. Proceedings of the Institution of Mechanical Engineers, Part L: Journal of Materials: Design and Applications, 229(3), 236-260. https://doi.org/10.1177/1464420713509699
9. Alipour, M.M., Shariyat, M., Shaban, M. (2010). A semi-analytical solution for free vibration of variable thickness two-directional-functionally graded plates on elastic foundations. International Journal of Mechanics and Materials in Design, 6(4), 293-304. https://doi.org/10.1007/s10999-010-9134-2
10. Amir, M., Lim, J., Kim, S.W., Lee, S.Y. (2023). Finite element analysis of natural frequencies of the FGM porous cooling plate with cutouts: a multilayered FGM approach. Results in Engineering, 20, 101532. https://doi.org/10.1016/j.rineng.2023.101532
11. Bellifa, H., Benrahou, K.H., Hadji, L., Houari, M.S.A., Tounsi, A. (2016). Bending and free vibration analysis of functionally graded plates using a simple shear deformation theory and the concept the neutral surface position. Journal of the Brazilian Society of Mechanical Sciences and Engineering, 38(1), 265-275. https://doi.org/10.1007/s40430-015-0354-0
12. Benferhat, R., Hassaine Daouadji, T., Hadji, L., Said Mansour, M. (2016). Static analysis of the FGM plate with porosities. Steel and Composite Structures, 21, 123-136. https://doi.org/10.12989/scs.2016.21.1.123
13. Jafari Mehrabadi, S., Kargarnovin, M.H., Najafizadeh, M.M. (2009). Free vibration analysis of functionally graded coupled circular plate with piezoelectric layers. Journal of mechanical science and technology, 23(8), 2008-2021. https://doi.org/10.1007/s12206-009-0519-9
14. Mahmoudi, A., Benyoucef, S., Tounsi, A., Benachour, A., Adda Bedia, E.A., Mahmoud, S.R. (2019). A refined quasi-3D shear deformation theory for thermo-mechanical behavior of functionally graded sandwich plates on elastic foundations. Journal of Sandwich Structures & Materials, 21(6), 1906-1929. https://doi.org/10.1177/1099636217727577
15. Hamza Madjid, B., Bouderba, B. (2023). Buckling analysis of FGM plate exposed to different loads

conditions. Mechanics Based Design of Structures and Machines, 51(12), 6798-6813. https://doi.org/10.1080/15397734.2022.2068576
16. Yang, E.C., Zhao, X., Li, Y.H. (2015). Free vibration analysis for cracked FGM beams by means of a continuous beam model. Shock and Vibration, 2015(1), 197049. https://doi.org/10.1155/2015/197049
17. Twinkle, C.M., Pitchaimani, J. (2021). Free vibration and stability of graphene platelet reinforced porous nano-composite cylindrical panel: Influence of grading, porosity and non-uniform edge loads. Engineering Structures, 230, 111670. https://doi.org/10.1016/j.engstruct.2020.111670
18. Chedad, A., Elmeiche, N., Hamzi, S., Abbad, H. (2022). Effect of porosity on the thermal buckling of functionally graded material (FGM) sandwich plates under different boundary conditions. Mechanics Based Design of Structures and Machines, 52(3), 1414-1436. https://doi.org/10.1080/15397734.2022.2148691
19. Jabbari, M., Hashemitaheri, M., Mojahedin, A., Eslami, M.R. (2014). Thermal buckling analysis of functionally graded thin circular plate made of saturated porous materials. Journal of thermal stresses, 37(2), 202-220. https://doi.org/10.1080/01495739.2013.839768
20. Fouda, N., El-midany, T., Sadoun, A.M., (2017). Bending, buckling and vibration of a functionally graded porous beam using finite elements. Journal of Applied and Computational Mechanics, **3**, 274-282. https://doi.org/10.22055/jacm.2017.21924.1121
21. Cottrell, J.A., Reali, A., Bazilevs, Y., Hughes, T.J. (2006). Isogeometric analysis of structural vibrations. Computer methods in applied mechanics and engineering, 195(41-43), 5257-5296. https://doi.org/10.1016/j.cma.2005.09.027
22. Van Do, V.N., Lee, C.H. (2019). Free vibration analysis of FGM plates with complex cutouts by using quasi-3D isogeometric approach. International Journal of Mechanical Sciences, 159, 213-233. https://doi.org/10.1016/j.ijmecsci.2019.05.034
23. Al-Furjan, M.S.H., Safarpour, H., Habibi, M., Safarpour, M., Tounsi, A. (2022). A comprehensive computational approach for nonlinear thermal instability of the electrically FG-GPLRC disk based on GDQ method. Engineering with Computers, 38(1), 801-818. https://doi.org/10.1007/s00366-020-01088-7
24. Vu, T.V., Cao, H.L., Truong, G.T., Kim, C.S. (2023). Buckling analysis of the porous sandwich functionally graded plates resting on Pasternak foundations by Navier solution combined with a new refined quasi-3D hyperbolic shear deformation theory. Mechanics Based Design of Structures and Machines, 51(11), 6227-6253. https://doi.org/10.1080/15397734.2022.2038618
25. Bui, T.Q., Nguyen, M.N. (2011). A novel meshfree model for buckling and vibration analysis of rectangular orthotropic plates. Structural engineering and mechanics, 39(4), 579-598. https://doi.org/10.12989/SEM.2011.39.4.579
26. Zenkour, A.M., Mashat, D.S. (2010). Thermal buckling analysis of ceramic-metal functionally graded plates. NS 02, 968-978. https://doi.org/10.4236/ns.2010.29118
27. Al-Furjan, M.S.H., Yang, Y., Farrokhian, A., Shen, X., Kolahchi, R., Rajak, D.K. (2022). Dynamic instability of nanocomposite piezoelectric-leptadenia pyrotechnica rheological elastomer-porous functionally graded materials micro viscoelastic beams at various strain gradient higher-order theories. Polymer Composites, 43(1), 282-298. https://doi.org/10.1002/pc.26373
28. Ni, Y., Tong, Z., Rong, D., Zhou, Z., Xu, X. (2018). Accurate thermal buckling analysis of functionally graded orthotropic cylindrical shells under the symplectic framework. Thin-Walled Structures, 129, 1-9. https://doi.org/10.1016/j.tws.2018.03.030
29. Joueid, N., Zghal, S., Chrigui, M., Dammak, F. (2024). Thermoelastic buckling analysis of plates and shells of temperature and porosity dependent functionally graded materials. Mechanics of Time-Dependent Materials, 28(3), 817-859. https://doi.org/10.1007/s11043-023-09644-6
30. Turan, M., Adiyaman, G. (2024). Free vibration and buckling analysis of porous two-directional functionally graded beams using a higher-order finite element model. Journal of Vibration Engineering & Technologies, 12(1), 1133-1152. https://doi.org/10.1007/s42417-023-00898-5
31. Yıldız, T., Esen, I. (2023). Effect of foam structure on thermo-mechanical buckling of foam core sandwich nanoplates with layered face plates made of functionally graded material (FGM). Acta Mechanica, 234(12), 6407-6437. https://doi.org/10.1007/s00707-023-03722-z

32. Wattanasakulpong, N., Ungbhakorn, V. (2014). Linear and nonlinear vibration analysis of elastically restrained ends FGM beams with porosities. Aerospace Science and Technology, 32(1), 111-120. https://doi.org/10.1016/j.ast.2013.12.002
33. Hadji, L., Madan, R., Bernard, F. (2024). Thermal buckling in multi-directional porous plates: The effects of material grading and aspect ratio. Proceedings of the Institution of Mechanical Engineers, Part G: Journal of Aerospace Engineering, 238(4), 412-426. https://doi.org/10.1177/09544100241232132
34. Javaheri, R., Eslami, M.R. (2002). Thermal buckling of functionally graded plates based on higher order theory. Journal of thermal stresses, 25(7), 603-625. https://doi.org/10.1080/01495730290074333